UNIVERSITY OF TARTU

Faculty of Science and Technology (LTT)

Institute of Physics

Andy Reiu

Classification of urban areas from Sentinel-1 coherence maps

Bachelor's thesis (12 ECTS)

Supervisors:
Karlis Zalite PhD
Kaupo Voormansik PhD

Tartu 2017

Contents

Abbreviations

C-Band Range of frequencies from 4 to 8 GHz. 9

ESA European Space Agency. 11

HH Horizontal transmit, horizontal receive. 8

HV Horizontal transmit, vertical receive. 8

InSAR Interferometric synthetic aperture radar. 5

S1TBX Sentinel-1 Toolbox. 11

SAR Synthetic aperture radar. 5

SLC Single look complex. 11

SRTM Shuttle radar topography mission. 16

UTC Coordinated universal time. 11

VH Vertical transmit, horizontal receive. 8

VV Vertical transmit, vertical receive. 8

1 Introduction

In today's developing world there is an ever growing increase in demand for more detailed information. One of the best ways in order to get fast and detailed information is using satellite imagery. It can be seen to have an important role in the decision making and developing process in a variety of industries. Urban mapping has also become more important with the growing global population, where major problems start to occur around metropolitan areas. This is particularly prominent in developing countries. Similar problems can also be seen in Estonia around Tallinn, where there is also increasing need for high-quality spatial data and a more effective way to improve the overall information.

It is estimated that 54 % of the world population live in the urban areas and the percent has been increasing steadily [1]. Urbanization has brought forth many serious problems, such as environmental pollution, traffic congestion and the destruction of natural resources [2]. Detailed mapping, coupled with better city planning, would help to lessen the side effects of the urbanization [3]. There are many solutions that might solve these problems, such as using satellite imagery.

Satellite imagery have been used for a long time and their importance has only increased in today's information society. The ever growing need for accurate imagery data brings out the need for new technology and techniques. It has brought out new ways on data gathering, such as Sentinel satellites launched by Copernicus program. Sentinel-1 satellites have already been used to study built-up areas. For example Kalev Koppel has used speckle divergence and repeat-pass interferometric coherence for the classification of built-up areas [4]. Similar research on built-up areas have also been done by Anni Sisas [5] and by Eva-Maria Tõnson [6]. This study provides a comparison to the urban area detection and classification with coherence method.

The main aim of this thesis is to calculate interferometric coherence from Sentinel-1 satellite image datasets to see how accurately we can register urban areas depending on different conditions, such as time separation and geometry. Coherence is calculated using two acquisitions. Time separation can be defined as time between the first image acquisition and second image acquisition. Sentinel-1 imagery are acquired during ascending and descending orbits over the study area in Tallinn. For calculating the accuracy of the method and detection of the urban buildings we use reference data from Republic of Estonia Land Board [25].

Following hypothesis where made:

- Time separation of the image acquisitions were taken as 1 year for 4 image sets and 3 months for 2 image sets. Hypothesis was made was that 3 month acquisitions will lead do a more accurate classification results than 1 year image sets.

- Classification accuracy varies depending whether the acquisitions were made during winter or summer.
- Accuracy differs with acquisition geometry.

This thesis is organized into 5 chapters. Theoretical background, which includes description of synthetic aperture radar (SAR) and interferometric synthetic aperture radarInSAR. Second chapter has the information about the main data and the study area. Chapter third gives an overview of the work-flow and how accuracy was described and calculated. Third chapter describes the conditions of the data and its study area. Discussion is in the fourth chapter. Final chapter is conclusion and recommendations for future research.

2 Theory

2.1 SAR principles

The following section gives an overview of the necessary theory in remote sensing and SAR principles. Publication [8] gives a more detailed overview on SAR.

SAR is an imagining radar mounted on a moving platform [9]. Electromagnetic waves are sequentially transmitted towards the earth surface. The reflected echoes are then received and stored by the radar antenna for further processing. In the case for SAR, its transmission and reception occurs at different times. Combination of the received backscattered signals allows to build a virtual aperture (form an image) that is much longer than the physical length of antenna. Thus giving it a name 'synthetic aperture'. This allows high azimuth resolution in the images despite the physically small antenna [10].

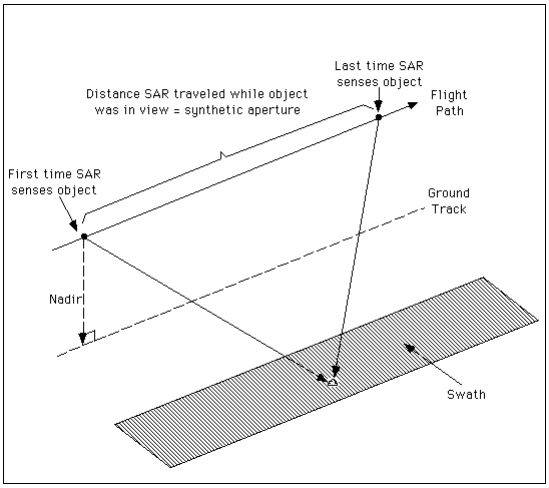

Figure 1: Image taken from ESA earth online and modified [7]. Moving platform synthesizes a large aperture, by recording the backscattered signals over the flight path.

The two spatial resolutions for SAR are range and azimuth resolutions, they are different from azimuth and range direction. For example range resolution depends on bandwidth. The azimuth resolution, due to the moving platform causing Doppler shift, depends on the antenna length in the along-track direction [12].

In order to image the terrain the platform needs to be based on steady flight (constant speed and altitude). The forward moving platform scans the earth along the track. Signal is then transmitted perpendicular to the track direction, down towards the target area. The beam is wide in the vertical direction, thus intersection on the surface of the beam is an oval shape with the long axis extending in the range direction. The backscattered

signals are received from the surface points at increasing range [13]. Side looking image configuration is illustrated in the Figure 2.

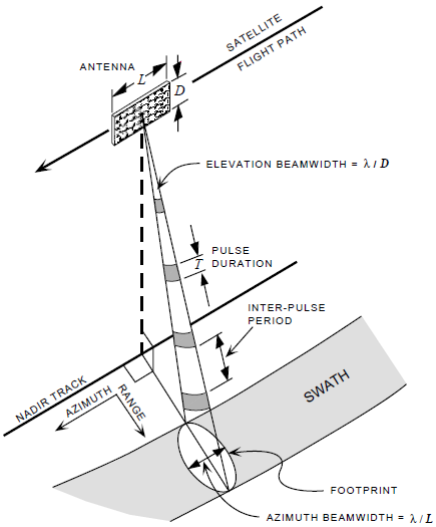

Figure 2: Image taken from Scientific SAR User's Guide [13], illustrates the typical scanning figure of a SAR system. Where a platform is moving along a track of azimuth direction and its slant range direction is perpendicular to the flight path.

The orbit in which the satellite is travelling is called either ascending or descending orbit. If it travels from south towards the north pole it's called ascending orbit. Conversely, if it travels the other way it is called descending orbit. For Sentinel-1 satellites, the antenna is fixed, thus descending orbit observes from east, and ascending passes observe from the west [16]. In Estonia descending images are acquired in the morning and ascending images in the afternoon.

SAR systems uses microwaves for remote sensing. Microwaves are good because of its ability to penetrate clouds, precipitation or some media, such as tree crowns. The penetration power increases for longer wavelengths - longer wavelength have a stronger penetration into vegetation and soil. Hence, using longer wavelength is more useful for urban study where the transitions are bigger and smaller wavelength for forest areas [19]. The backscattered signals intensity increases with the surface roughness, which depends on the wavelength that was used. If the surface appears rough, it appears brighter in the radar image due to its backscattered signal from the surface [11]. Surface roughness depends on the wavelength of radar. For Sentinel-1 the wavelength is 5.5 cm[22]. In this study roughness is insignificantly small, because of the relatively large wavelength.

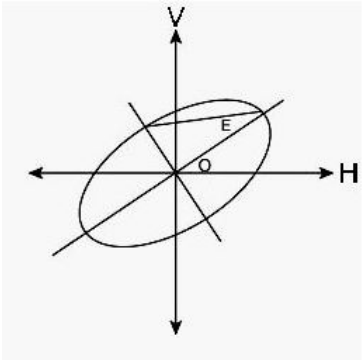

Figure 3: Illustrates electromagnetic polarization of an electromagnetic wave horizontal (H) and vertical (V).

SAR system can simultaneously transmit and receive both horizontal (H) and vertical (V) electric field vectors. If EM wave oscillates along the parallel to horizontal direction, it's called „H“ polarized. On the other hand, if its oscillation is vertical it's called „V“ polarized. After the interaction with the object the polarization may change. Hence, the backscattered signal might consist of the two polarizations. This allows synthesizing images with four different configurations: VV (vertical transmitting, vertical receiving), HH (horizontal transmitting, horizontal receiving) or HV (horizontal transmitting, vertical receiving) polarizations, VH (vertical transmitting, horizontal receiving) [15]. Oscillation of “H“ and “V” can be seen in Figure 3.

The backscatter depends on polarization. Generally artificial surfaces, such as buildings, are good scatters of VV and HH, because of their parallel and vertical walls with the flight path. VH and HV accuracy would be higher if the building walls and satellite make a 45°angle, but its energy is more scattered [14]. Sentinel-1 Single Look Complex (SLC) products are available only in VV and VH polarization. VH has a lower backscatter, thus this study uses only VV polarization.

After the signal has backscattered from the targets surface it will have lost a proportion of its energy. This is due to the multiple reasons, such as physical factors. For example backscatter depends on dielectric properties and moisture of the surface material. Wetter targets appear bright and dry targets appear darker. Backscatter is also affected by target's orientation towards the radar line of sight. Frequency and polarization of a SAR system will also have an affect on the backscatter [20].

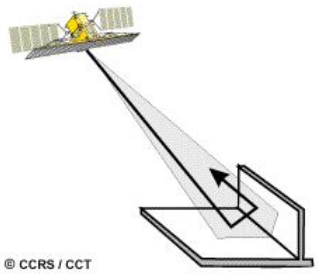

Figure 4: Illustrates corner reflection.

Surfaces will have stronger backscatter if they are inclined towards radar; two such planes make a corner, which is called as corner reflection. Where the corners will appear brighter in the image. Hence, urban environments (e.g. buildings, streets) will appear as very bright targets in the image (see Figure 4). On the other hand some of the taller targets can block the signal, thus the area blocked will appear dark in the image [20].

2.2 SAR interferometry

Interferometric Synthetic Aperture Radar (InSAR) is a radar technique that is used in remote sensing. It uses two or more SAR images to generate maps of digital elevation, surface deformation or do measure the coherence of two images. The technique uses the measurement of signal phase change over a period of time [17]. Interferometric coherence (γ) of two complex SAR images can be defined as:

$$\gamma = \frac{\mid \nu_1 \nu_2^* \mid}{\sqrt{|\nu_1|^2 |\nu_2|^2}} \tag{1}$$

where γ is the value of the coherence at certain pixel, ν_1 and ν_2 are the complex SAR images, * is complex conjugate of the other image [18].

The complex correlation coefficient gamma (Formula 1) can be split up into two factors: amplitude (coherence) and phase. The study measures the coherence of observed target over the time between two acquisitions. For example if a field has been ploughed or tree leaves have fallen, the areas show a decorrelation in the analysis. This technique can also be used to monitor changes in infrastructure, where study presumes that buildings don't change over time [18].

Coherence can have values between 0 to 1. When the target has not changed over time the coherence is close to 1. Otherwise if it decorrelates it has a value near 0.

2.3 Sentinel-1

In the thesis Sentinel-1 satellite imagery was used. The satellite sends and receives signals in C-Band, which operates at a center frequency of 5.405 GHz [21].

Sentinel-1A was launched by European Space Agency within the Copernicus Programme at 3 April 2014, consisting of a constellation of two satellites, which are Sentinel-1A and Sentinel-1B (sent up at 25 April 2016). The two satellites orbits are 180 °apart, which allows to map a image of the entire Earth in six days.

Sentinel-1 was designed to be reliable, providing for day-and-night, global coverage in all weather. This enables the development for new applications for mapping land surfaces.

In the following Table 1 technical parameters and chosen operating mode are given for the Sentinel-1 satellite [22].

Satellite	Sentinel-1
Centre Frequency (GHz)	5.405
Polarization	VV
Incidence angle range	29.1°- 46°
Swath Mode	Interferometric Wide swath (IW)
Swath width(km)	250
Spatial resolution (single look)(m)	5×20
Product used	Level-1 SLC Product

Table 1: Key parameters and chosen operating mode for Sentinel-1 C-SAR. [22]

3 SAR images and study area

3.1 Satellite imagery

Sentinel-1 satellite images, which was funded by European Union and was carried out by the ESA in Copernicus Programme. They are provided for free and open accessed in online site - Copernicus Open Access Hub.

The study uses Level-1 Single Look Complex (SLC) products with VV polarization. The product consists of focused SAR data in the slant range geometry, with phase and amplitude information [22]. Product size is around 4.2 GB. Research was done on both ascending and descending images with time separation of both 3 months and 1 year. This includes images taken during summer and winter. The coherence was measured and processed through Sentinel-1 toolbox (S1TBX), which was developed by the European Space Agency [26].

Satellite images that were used are shown in the following Table 2 and Table 3. They include the following information: radar image time that it was taken, time when they where taken in Universal Time Coordinated (UTC), orbit and the incidence angle.

Date	Time	Orbit	Incidence angle
2016-07-01	15:56:21	Ascending	24°40' -24°52'
2015-07-07	15:56:20	Ascending	24°40' -24°52'
2016-07-08	04:33:31	Descending	24°55' -24°36'
2015-07-02	04:33:36	Descending	24°55' -24°36'
2016-08-30	15:56:28	Ascending	24°40' -24°52'
2016-06-07	15:56:22	Ascending	24°40' -24°52'

Table 2: Sentinel-1 SLC Satellite images taken during summer.

Date	Time	Orbit	Incidence angle
2016-01-10	04:33:30	Descending	24°55' -24°36'
2015-01-03	04:33:35	Descending	24°55' -24°36'
2017-01-04	04:33:31	Descending	24°55' -24°36'
2016-01-10	04:33:36	Descending	24°55' -24°36'
2017-02-26	15:56:22	Ascending	24°40' -24°52'
2016-12-04	15:56:20	Ascending	24°40' -24°52'

Table 3: Sentinel-1 SLC Satellite images taken during winter.

The image pairs that were used during the thesis, both ascending and descending can be seen in the Table 3 as corresponding series of pairs. Coherence estimation needs image pairs. These image pair combinations will be used in the work-flow process.

Sentinel-1 can receive and send data during any weather but as was mentioned in Section 2.1 humidity has an significant change on the electric properties of surface materials, lowering its coherence. In the final results this will be taken into account. In the next Table 4 weather conditions for the satellite images can be seen; radar image date, time, precipitation in the previous day and temperature during the time the image was taken. The weather conditions were taken from Estonian Weather Service around Tallinn-Harku [23].

Radarimage date	Time (UTC)	Precipitation (mm)	Temperature (°)
2016-01-10	04:33:31	0	-20.8
2015-01-03	04:33:35	0	0.7
2017-01-04	04:33:31	0	-8.5
2016-01-10	04:33:36	0	-20.8
2017-02-26	15:56:22	0	0.7
2016-12-04	15:56:20	0	-3.3
2016-07-01	15:56:21	0	21.4
2015-07-07	15:56:20	0.3	14.5
2016-07-08	04:33:31	1	12.6
2015-07-02	04:33:36	0	12.6
2016-08-30	15:56:28	0	14.8
2016-06-07	15:56:22	0	18.4

Table 4: Tallinn-Harku weather conditions

3.2 Study area

The 17×20 km^2 study area is located in Tallinn, capital of Estonia. Population of Tallinn as of 2017 1st March is around 444 200 [24]. The area was selected because of its fast growth in Estonia, and therefore having increasing population and change of landscape.

The reference data for the land cover classes were taken from the Estonian Land Board's topographical database[25].

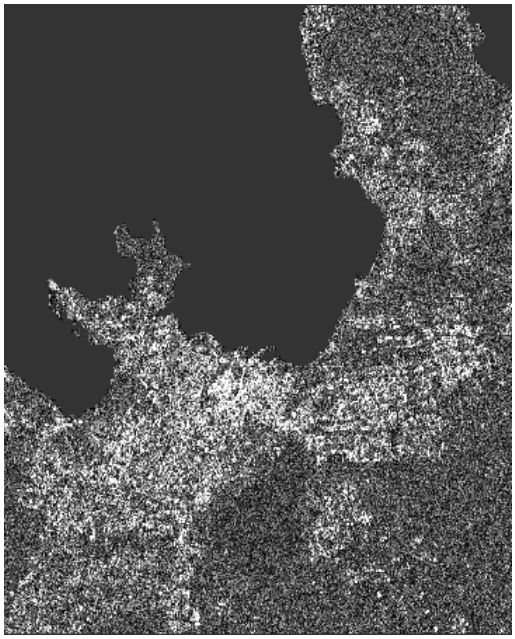

Figure 5: Coherence image of the study area.

4 Radar image processing

The Sentinel-1 SLC products were processed using Sentinel-1 Toolbox (S1TBX) version 5.0.0. [26]. The process of analyzing the images can be seen in the work-flow chart steps from figure 6.

1. Reading data

   SLC products were opened and read using Sentinel-1 toolbox.

2. Co-registration

   In order to combine two images that were taken at different points in time and altitude, the images need to be co-registered. This method is used mostly for InSAR processing. Images need to have same polarization and projection system. For each data set the first image was considered as the master scene and the next taken image as slave scene that will be co-registered to the master. This will superimpose the slant range geometry with each data set.

   The images were first split into 3 sub-swaths. Sub-swath which consist of the study area was selected, this was in order to make the processing faster. The co-registration was done using "S1 TOPS Co-registration" with operator "S1 Back Geocoding".

3. Coherence estimation

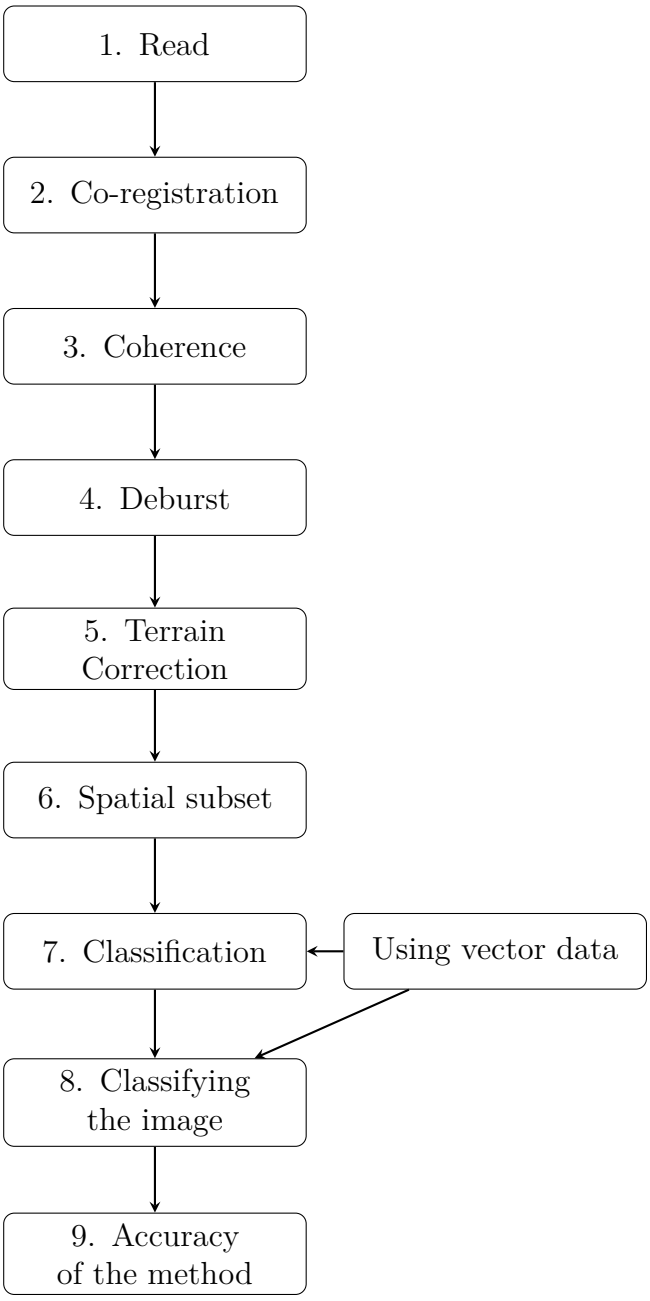

Figure 6: Workflow graph

The coherence estimation was made according to Section 2.2. To remove the estimation bias for averaged sample, a window of azimuth 3 and range 9 was used [29].

4. Deburst

   Acquisition mode of S1 produces bursts or subsets of swath. In order do merge them into one continuous image de-burst is needed. De-bursting was done with VV polarization.

5. Terrain-correction

   Next step is using Terrain-correction to project the data from radar to ground coordinates. It was done using function Terrain correction, with an digital elevation model SRTM 3 sec and using bilinear interpolation with a coordinate system EPSG:3301 - Estonian Coordinate system of 1997.

6. Selecting spatial subset

   After terrain correction a smaller subset of the study region was created. The center of the study area was Tallinn. See section 3.2 for the study area.

7. Classification

   In order to classify the image into urban and non-urban areas, two masks need to be created. This was done by using Sentinel-1 toolbox operator mask manager, were different masks can be created. Urban mask was directly created by using the vector data, this includes all pixels inside the mask. Second mask was made to estimate the pixels that were outside the urban mask, thus named non-urban mask.

8. Classifying the images

   Histograms of urban and non-urban classes were computed and the overlap of between the histograms of the two classes was compared. Histograms for the given non-urban areas and for urban areas can be seen in the following Figure 7.

Comparing the histograms of non-urban and urban areas, threshold value was selected. Its value depends on the overlap of non-urban and urban classes. This method of selecting threshold is called bimodal method [28]. After the threshold was selected a new coherence image was created. It compares the coherence values found in the image with the selected threshold, if the value was larger then the threshold was set to one, if it was smaller then it was set to zero. Next was computing of both masks and comparison of the urban and non-urban areas.

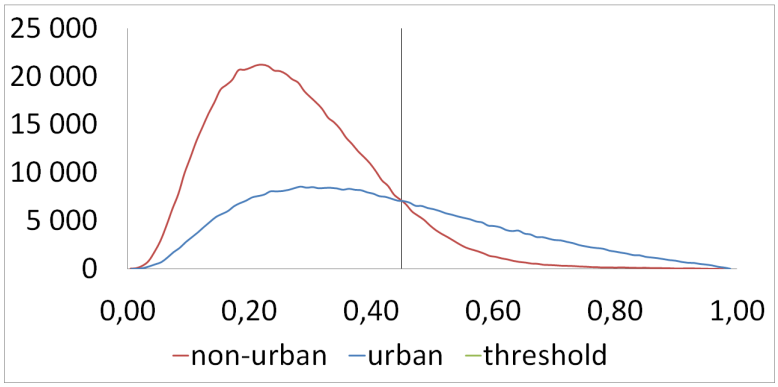

Figure 7: Histograms of non-urban and urban areas and the selected threshold value that was used for the binary mask, example was taken from 26.02.2017-04.12.2016 image set.

4.1 Accuracy of the method

Classification of accuracy was calculated using the confusion matrix method. This method can give a detailed analysis over the classification - accuracy of the method and correctly classified classes [27].

$$ACC = \frac{TP + TN}{P + N} \tag{2}$$

ACC is confusion matrix accuracy; TP is the correctly found urban areas, TN is the correctly found non-urban areas, which were correctly found and $P + N$ is sum of all pixels (total number of predictions) [27].

4.2 Correctly classified buildings

Correctly classified buildings can be defined as:

$$B = \frac{TP}{FP + TP} \tag{3}$$

Where B is the correctly classified buildings. TP is the correctly found buildings that where detected and FP is the non-built areas that were classified as buildings [27].

5 Results and discussion

The study analyzed 6 image sets with different orbit and time separation, using VV polarization. This includes both ascending and descending orbits. The time of the acquisitions was taken as winter and summer. The process analyzed the histograms, accuracy of the method and correctly classified buildings.

Date	Season	Orbit	Accuracy(%)	Precision(%)
26.02.2017-04.12.2016	Winter	ASC	70	71.4
30.08.2016-07.06.2016	Summer	ASC	72.3	73.2
01.07.2016-07.07.2015	Summer	ASC	71.1	73.3
10.01.2016-03.01.2015	Winter	DESC	65.5	66.5
04.01.2017-10.01.2016	Winter	DESC	67.4	70.5
08.07.2016-02.07.2015	Summer	DESC	69.6	73.7

Table 5: Table shows the values from the images that were taken and processed, orbit, the accuracy of the method (accuracy) and the correctly found buildings (precision), the values were calculated through confusion matrix.

Comparing orbits with accuracy we can see that the ascending orbits yield higher results and higher accuracy of the method than descending orbits. For example image pairs of 08.07.2016 and 02.07.2015, which were descending orbits, gives us an accuracy of 69.6%, comparing it to 01.07.2016 and 07.07.2015, which has an higher accuracy of 71.1%. The changes can be cause by the varying conditions during morning and night. Descending acquisitions were done at early mornings and ascending acquisitions was done in the afternoon. In the morning the moisture can condense dew or frost, depending on the temperature.

Table 5 also shows that winter data yields lower accuracy of classification and accuracy of the correctly found buildings than summer images. This can be seen by comparing results of the image pairs of 04.01.2017-10.01.2016 and 08.07.2016-02.07.2015. Both image sets use same orbit, winter image pairs correctly found buildings out of 70.5% time, summer image pairs found correct buildings 73.7% of time. By comparing the histograms of winter and summer in the Figure 9 and Figure 10, there is a slight difference of coherence in the range 0.50 to 1 - slight decrease per pixel for urban areas in winter. This coherence change can be assumed to be caused by snow, thus giving it a different scattering property. Assumption was made by using the weather data in Table 4.

Figure 8 shows the accuracy of the method of time separation 1 year and 3 months during winter and summer. Winter image pairs with time separation of 1 year are from 10 January 2016 - 03 January 2015, 3 months are from 26 February 2017 - 04 December 2016. Summer image pairs with time separation of 1 year are from 01 July 2016 – 07 July 2015, time separation of 3 months are from 30 August 2016 – 07 June 2016. Accuracy of the method is compared with the time separation between the images.

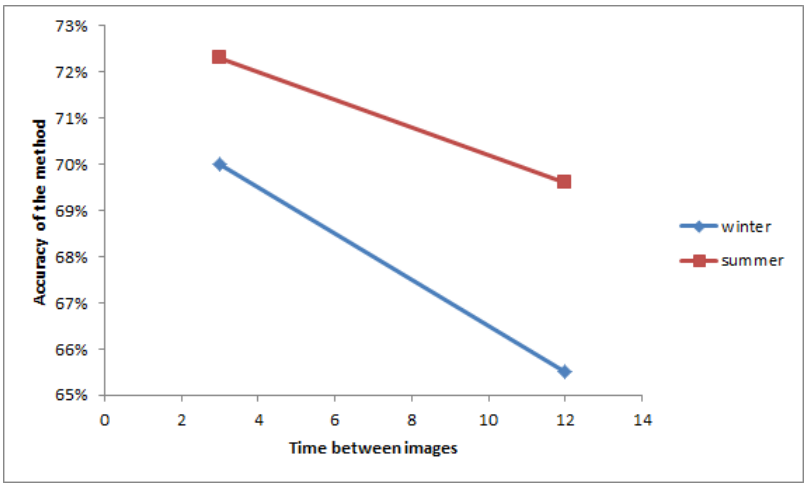

Figure 8: Results of the time difference between 3 months and 1 year, taken during winter and summer. Acquisitions are given on the x-axis and y-axis shows the accuracy of the method.

In the Figure 8, one of the important points that can be derived is that the accuracy of the coherence lowers with respect to the time between the images. This result can be seen in the accuracy of 3 months, which is 72.3 % and for 12 months it is 69.6%. Similar results can also be seen for the winter data as its accuracy for 3 months is 70% and 12 months is 65.5%. Thus we can assume that longer time intervals lead to lower coherence; this is caused by the temporal decorrelation of the signal. The overall coherence is affected by temporal baselines, changes over time.

	08.07.2016 - 02.07.2015			10.01.2016 -03.01.2015		
	N-Urban	Urban	Total	N-Urban	Urban	Total
N-Urban	624722	284819	909541	626646	332834	959480
Urban	52810	148251	201061	50527	100166	150693
Total	677532	433070	1110060	677173	433000	1110173
	30.08.2016 - 07.06.2016			04.01.2017 - 10.01.2016		
N-Urban	605235	235495	840730	625252	310406	935658
Urban	72411	197610	270021	51353	122659	174012
Total	677646	433105	1110751	676605	433065	1109670
	01.07.2016 - 02.07.2015			26.02.2017 - 04.12.2016		
N-Urban	624722	284819	909541	610080	266188	876268
Urban	52810	148251	201061	66964	166943	233907
Total	677532	433070	1110602	677044	433131	1110175

Table 6: Accuracy of the classification was calculated using confusion matrix method (Section 4.1).

Table 6 shows the confusion matrix table. It consist of two rows and two columns. Column in the table represents ground truth classes, while each row represents classes of the classified image. Cells show the possible correlation between the ground data and the classification. Separately they are called as true positives, true negatives, false positives and false negatives [30]. Table 6. has been separated into left columns were confusion matrix values are from the summer data and right side columns which consist of winter data. Total number of pixels can be seen in the right down most corner for each image sets. Non-urban is written as 'N-urban'.

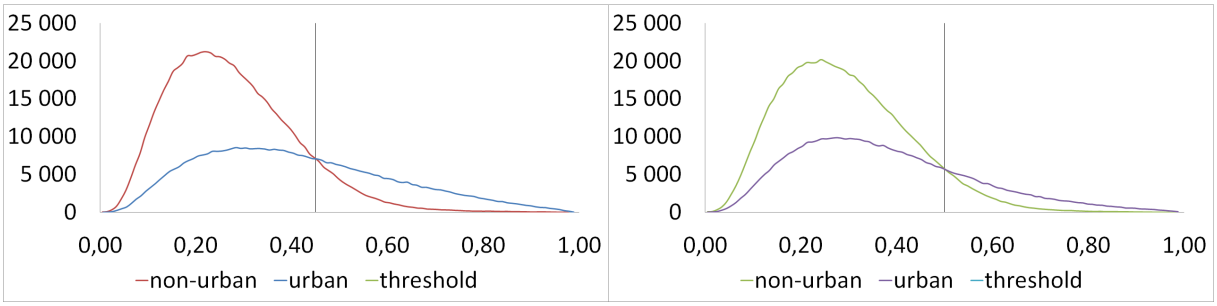

(a) 26.02.2017-04.12.2016

(b) 10.01.2016-03.01.2015

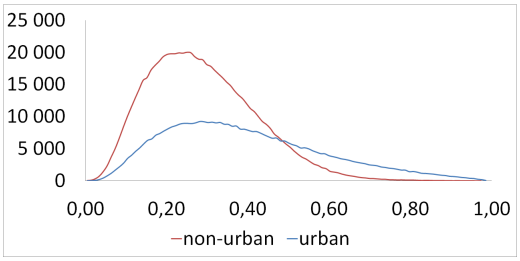

(c) 04.01.2017-10.01.2016

Figure 9: Graphs show the histograms of non-urban and urban areas at winter time. Y-axis shows the pixel percentage in the areas. X-axis shows the interferometric coherence value.

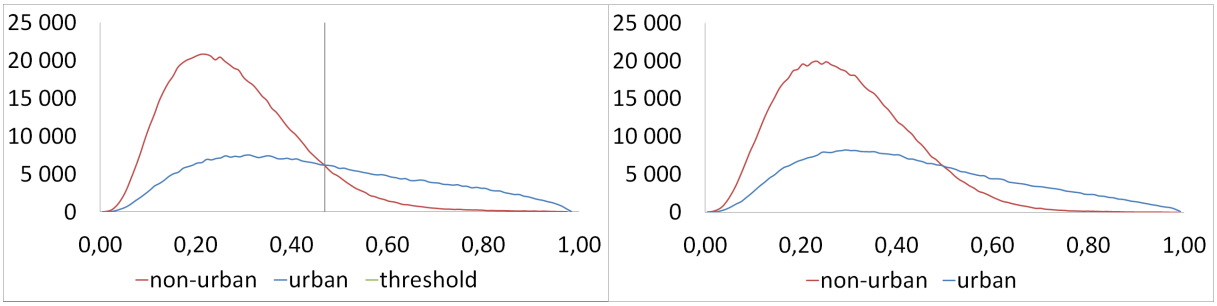

(a) 30.08.2016-07.06.2016

(b) 08.07.2016.02.07.2015

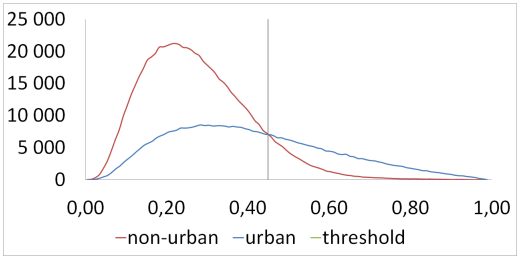

(c) 01.07.2016-07.07.2015

Figure 10: Graphs show the histograms of non-urban and urban areas at summer time. Y-axis shows the pixel percentage in the areas. X-axis shows the interferometric coherence value.

.

In the Figure 9 and Figure 10. The overlap in the range of 0 - 0.5, shows that urban pixels have low coherence values. This can be explained that urban areas have detected other backscatter, which have a lower coherence value. Such as vegetation (trees in yards), streets. It can also be cause by the temperature and the humidity when the image was taken.

6 Conclusion

The aim of this study was to see how precisely urban areas can be mapped using interferometric coherence on Sentinel-1 satellite imagery with different conditions. These conditions include: time separation of 3 months and 1 year, ascending and descending orbits, winter and summer data. The images were processed through Sentinel-1 Toolbox with 9 steps (Figure 4). The chosen study area was Estonian capital city Tallinn and its surroundings (Figure 3). These results could further improve urban mapping and the detection of buildings.

The study uses Sentinel-1 image sets to measure image coherence. Another important part of the study was classification urban and non-urban areas. That would lead to time-saving improvements when using manually defined rules for building detection.

The main results of the study are:

- Results show that ascending orbits yield higher accuracy of the classification (71.1%) than descending orbits (69.9%). The comparison was made using 2015 and 2016 summer images sets. The reason for the cause is assumed to be the difference of early morning and afternoon weather conditions (Table 4).

- Accuracy can be improved by using summer images - winter data yields lower accuracy in correctly found buildings than summer images (Figure 8). This conclusion was made when same orbits were used - winter image pairs found buildings correctly 70.5% and for summer image the detection was 73.7%. Assumption was made using the weather data, that the areas contained snow, thus giving it a different scattering property and lowering the accuracy of winter data.

- Accuracy of the coherence lowers depending on the time of the image acquisitions - time separation of 3 months yields higher accuracy than 1 year. This conclusion was made after comparing two data sets for winter and summer. It is caused by the temporal correlation of the signal change over time.

These results could provide useful information for further mapping of urban areas with coherence method. Especially for SAR datasets that were used in this study.

Further continuation of this study can improve the accuracy and the quality of detecting urban areas. There are several key ways to improve the research. This could be done by making time separation of images down to 1 month or by combining with HH polarization.

Keywords: Urban areas, remote sensing, synthetic aperture radar, coherence, Sentinel-1

CERCS: T181 Remote sensing

7 Kokkuvõte

Äärelinnade klassifitseerimine Sentinel-1 koherentsi piltide põhjal

Töö eesmärk oli arendada interferomeetrilise koherentsuse meetodit ning selgitada välja, kui täpselt on võimalik uurida äärelinnade hoonestuste paiknemist erinevates tingimustes. Koherentsuse meetodi arvutamiseks kasutati Sentinel-1 sateliidi pilte. Pildid olid tehtud talve ja kevade andmete põhjal, mis olid tehtud nii tõusval kui ka laskuval orbiidil. Pildiseeriate omavaheline aeg oli kolm kuud või üks aasta. Töös arendati välja üheksast sammust koosnev interferomeetrilise koherentsuse töötlusahel Sentinel-1 Toolbox abil (Joonisel 4). Uurimisustöö objektiks oli Tallinn ja Tallinna äärelinn (Joonis 3).

Töö käigus selgus, millistel tingimustel on parem linnapiirkondi klassifitseerida. Peamised tulemused on järgnevad:

- Töös võrreldi pilte, mis tehti nii tõusval kui ka laskuval orbiidil. Sentinel-1 tõusva orbiidi tulempiltide täpsus (71.1%) osutus kõrgemaks kui langeva orbiidi korral (69.9%). Võrdlus tehti 2015. ja 2016. aasta suve piltide põhjal. Järeldati, et erinevuse põhjuseks on erinev ilmastikutingimus. Langeva orbiidi pildid on tehtud varahommikul, kus võib olla udu ja härmatis aga tõusva orbiidi pildid olid tehtud peale lõunat (Tabel 4).

- Meetodi täpsus paranes, kui kasutada suvel tehtud pilte, kuna talve piltide andmed andsid madalama täpsuse. Samal orbiidil tehtud piltide korral leidis talve seeriast ehitised 70.5% juhtudest ja suve pildi seeriast 73.7% juhtudest. Võib järeldada, et see on põhjustatud samuti ilmastikutingimustest. Talvel oli maa kaetud lumega ning seetõttu oli maapinnal teistsugused elektrilised omadused.

- Koherentsi täpsuse väärtus langes, mida suurem oli piltide omavaheline aeg - ajavahemik kolm kuud andis suurema täpsuse kui ajavahemik üks aasta. Järeldus tehti suve ja talve pildiseeriate võrdlemisel. Koherentsi languse põhjustas ajaline korrelatsioon.

Tulemused annavad kasulikku informatsiooni äärelinnade hoonestuse edaspidiseks uurimiseks koherentsuse meetodil.

Edaspidi võiks täpsemalt uurida, kuivõrd võib vähendada tulempiltide ajavahemikku nii, et täpsus kasvaks. Lisaks võiks kombineerida andmed HH polarisatsiooniga.

Märksõnad: linnapiirkonnad, kaugseire, tehisavaradar, koherents, Sentinel-1
CERCS: T181 Kaugseire

8 References

[1] Washington (2016). 2016 World Population Data Sheet. http://www.prb.org/Publications/Datasheets/2016/2016-world-population-data-sheet.aspx (01.04.2017).

[2] United Nations publication (2011). http://www.un.org/esa/population/publications/PopDistribUrbanization/PopulationDistributionUrbanization.pdf (01.04.2017).

[3] Champion, N.(2007). 2D building change detection from high resolution aerial images and correlation digital surface models. International Archives of Photogrammetry, Remote Sensing and Spatial Information Sciences. Vol. 36 (Part 3/W49A), Munich, Germany.

[4] Koppel, K., Zalite, K., Sisas, A., Voormansik, K., Praks, J., Noorma, M. (2015). Sentinel-1 for Urban Area Monitoring — Analysing Local-area Statistics and Interferometric Coherence Methods for Buildings' Detection. 2015 IEEE International Geoscience and Remote Sensing Symposium (IGARSS), 1175–1178.

[5] Sisas, A. (2015). Ehitiste tuvastamine radarsatelliidi Sentinel-1A mõõtmiste põhjal. http://dspace.ut.ee/handle/10062/48404 (01.04.2017).

[6] Tõnson, E.M. (2016). Hoonestatud alade tuvastamine ERS-2, Envisati ja Senintel-1 Tehisavaradarite andmetelt.

[7] European Space Agency. ESA. https://earth.esa.int/handbooks/asar/CNTR4.html (02.04.2017)

[8] Curlander, J. C. McDonough, R. N. (1991). Synthetic Aperture Radar: Systems and Signal Processing. New York.

[9] Moreira, A., Prats-Iraola, P.; Younis, M., Krieger, G., Hajnsek, I.; P. Papathanassiou, K. (2013). A tutorial on synthetic aperture radar. IEEE Geoscience and Remote Sensing Magazine. Volume: 1, Issue: 1.

[10] Shivakumar, R., Vincent, D., Jerome, L. N., Neal, P., Joel, G. (2002). Synthetic Aperture Radar Imaging Using Spectral Estimation Techniques. University of Michigan.

[11] Gomarasca, M. A.(2009). Basics of Geomatics. pp. 470.

[12] Rouyer, L., Lauknes, T. R., Hodga, K.-A. (2015). Spaceborne radar interferometry (InSAR) for natural hazards, landslides and infrastructure: limitations and potential. Northern research institute.

[13] Olmsted, C.(1993). Scientific SAR User's Guide. Alaska SAR Facility. https://media.asf.alaska.edu/asfmainsite/documents/sci-sar-userguide.pdf (16.04.2017)

[14] Raney, R.K. (1998). Radar fundamentals: technical perspective, in Principles and Application of Imaging Radar. Manual of Remote Sensing, Third Edition, Volume 2. John Wiley and Sons.

[15] Lin, S.-L.(2013). Introduction to Modern EW Systems. pp. 101-104. DOI: 10.3390/s130101146.

[16] Carrasco, D. , Díaz, J. , Broquetas, A. (2014). Combination of interferograms from ascending and descending orbits. IGARSS 94, Vol. 2, pp. 733-735. DOI: 10.1109/IGARSS.1994.399244.

[17] Hanssen, R. F. (2001). Radar Interferometry: Data Interpretation and Error Analysis. Netherlands, Kluwer. DOI: 10.1007/0-306-47633-9.

[18] Bamler, R., Just, D. (1993), Phase statistics and decorrelation in SAR interferograms. Geoscience and Remote Sensing Symp. IGARSS '93, vol.3, pp.980-984. DOI: 10.1109/IGARSS.1993.322637.

[19] Engdahl, M., Borgeaud, M., Rast, M. (2001). The use of ERS-1/2 Tandem interferometric coherence in the estimation of agricultural crop heights. IEEE Trans GARS. Vol. 39, N. 8, pp 1799–1806. DOI: 10.1109/36.942558.

[20] European Space Agency. ERS Radar Courses. https://earth.esa.int (02.04.2017)

[21] European Space Agency. ESA. http://www.esa.int (02.04.2017)

[22] European Space Agency. ESA Sentinel. https://sentinels.copernicus.eu (02.04.2017)

[23] Riigi Ilmateenistus. Weather conditions – Riigi Ilmateenistus. http://www.ilmateenistus.ee/ilm/ilmavaatlused/vaatlusandmed/ (01.04.2017).

[24] Tallinn (2002-2017). http://www.tallinn.ee/est/Tallinna-elanike-arv (01.04.2017).

[25] Maa-amet (2017). ETAK Vector data. http://geoportaal.maaamet.ee/est/ (01.04.2017)

[26] Sentinel Application Platform. http://step.esa.int/main/download/ (04.04.2017)

[27] Stehman, Stephen V. (1997). Selecting and interpreting measures of thematic classification accuracy. Remote Sensing of Environment. 62 (1): pp. 77–89. DOI:10.1016/S0034-4257(97)00083-7.

[28] Shen, H., Johnson, C. R. (2003). SemiAutomatic Image Segmentation: A Bimodal Thresholding Approach. Department of Computer Science University of Utah. USA.

[29] Touzi, R., Lopes, A., Bruniquel, J., Vachon, P.W. (1999). Coherence estimation for SAR imagery. Canada Centre for Remote Sensing, Ottawa, Ont., Canada. pp. 135 - 149. DOI: 10.1109/36.739146.

[30] Kohavi, R., Provost, F. (1998). Glossary of Terms. The Netherlands. DOI: 10.1023/A:1017181826899. http://ai.stanford.edu/ ronnyk/glossary.html (02.04.2017).

A First appendix: Processed study area

Figure 11: Processed study area

B Second appendix: Urban mask

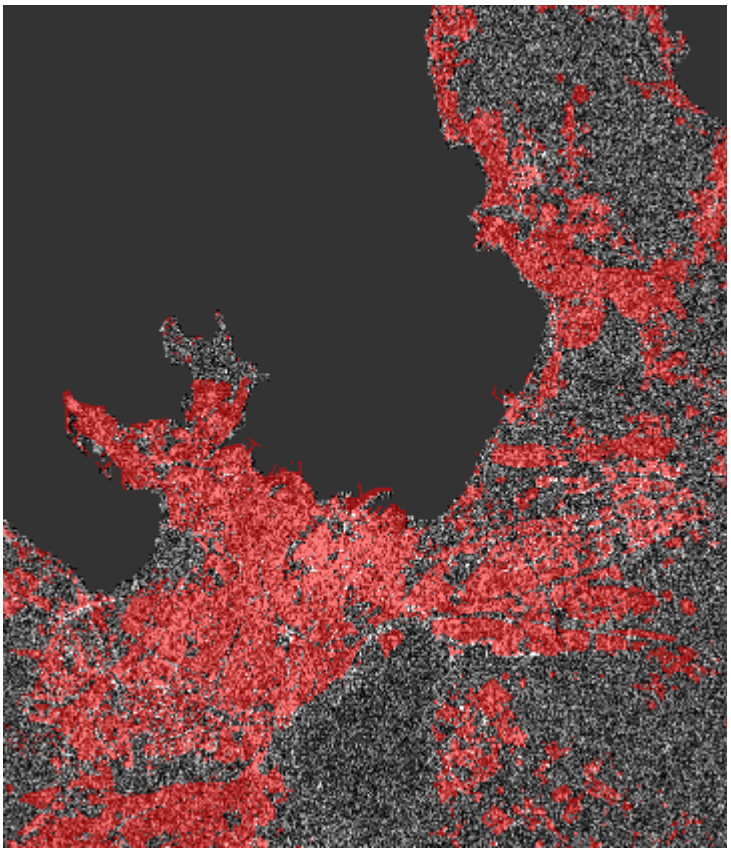

Figure 12: Urban mask on the study area

C Third appendix: Non-urban mask

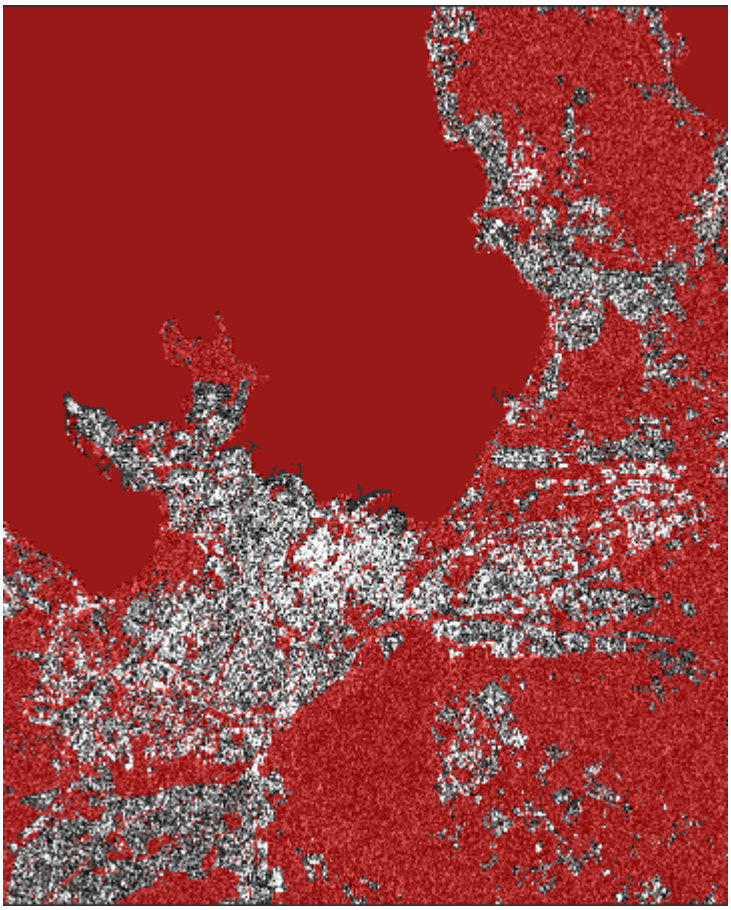

Figure 13: Non-urban mask on the study area

Lihtlitsents lõputöö reprodutseerimiseks ja lõputöö üldsusele kättesaadavaks tegemiseks

Mina, Andy Reiu,

1. Annan Tartu Ülikoolile tasuta loa (lihtlitsentsi) enda loodud teose

   Classification of urban areas from Sentinel-1 coherence maps,

   mille juhendajad on Karlis Zalite ja Kaupo Voormansik,

   (a) reprodutseerimiseks säilitamise ja üldsusele kättesaadavaks tegemise eesmärgil, sealhulgas digitaalarhiivi DSpace-is lisamise eesmärgil kuni autoriõiguse kehtivuse tähtaja lõppemiseni;

   (b) üldsusele kättesaadavaks tegemiseks Tartu Ülikooli veebikeskkonna kaudu, sealhulgas digitaalarhiivi DSpace'i kaudu kuni autoriõiguse kehtivuse tähtaja lõppemiseni.

2. Olen teadlik, et punktis 1 nimetatud õigused jäävad alles ka autorile.

3. Kinnitan, et lihtlitsentsi andmisega ei rikuta teiste isikute intellektuaalomandi ega isikuandmete kaitse seadusest tulenevaid õigusi.

Tartu, 25. mai 2017. a.